CHAPTER IV
EFFECTS OF SURFACTANT CONCENTRATIONS AND TYPES ON SYNTHESIZED POLYCARBAZOLE BY INTERFACIAL POLYMERIZATION

4.1 Abstract

Polycarbazole (PCB) was synthesized via interfacial polymerization method using carbazole monomer and ammonium persulfate (APS) as the oxidant. The effects of surfactant types (nonionic as TW20, cationic as CTAB, and anionic as SDS) and surfactant concentrations on the synthesized PCB were investigated based on the roles of micelle formation. The electron microscopy images revealed various PCB morphologies depending on the surfactant types and surfactant concentrations. The new morphological structures of the obtained PCB were macroporous honeycomb, connected hollow sphere and smaller hollow sphere depending on the surfactant types. The electrical conductivity values of the doped PCB synthesized with CTAB were the highest and higher than that without a surfactant by three orders of magnitude. The highest electrical conductivity of doped PCB_CTAB obtained was 11.3 S/cm.

Keywords: conducting polymer; polycarbazole; interfacial polymerization; electrical conductivity

4.2 Introduction

In recent years, electro-active conductive polymers are becoming more important because they can be applied as sensor materials (Kumar *et al.*, 2008 and Murat Ates, 2013), electrochemical transistors (Horowitz *et al.*, 1998 and Saxena *et al.*, 1998), solar cells (Ranger *et al.*, 1998), and etc. The most widely studied conductive polymers are polyaniline, polypyrrole, and polythiophene. Polycarbazole (PCB) is one of the electroactive conductive polymers, polymerized from carbazole monomer that consisting of two six-membered rings fused on a side of a five-membered nitrogen containing ring. Its conductivity has been shown to be more than

10^{-3} S/cm, the PCB can be synthesized by either electrochemical or chemical polymerization method (Gupta and Prakash *et al.*, 2010).

Recently, investigations on the PCB synthesis by both electrochemical and chemical methods have been carried out (Rani *et al.* 1998, Morin *et al.* 1998, and Tran-Van *et al.* 2002). Furthermore, the chemical synthesis method of PCB has been of interest because it is the most feasible route for the large scale production (Zhuo *et al.*, 2009). The PCB interfacial polymerization is one of chemical polymerization methods. It has been successfully used to synthesize three dimensional hollow microsphere of PCB (Gupta *et al.*, 2010). Moreover, surfactant-assisted chemical route is of particular interest because it can generate surfactant templates of various new shapes where they can be removed after polymerization (Gupta *et al.*, 2010). Polycarbazole spheres have been successfully synthesized via a hydrothermal method (Zhuo *et al.*, 2013). Polyvinylpyrrolidione was used as the template. The synthesis was simple, it improved the electrical conductivity, was of low cost and environment friendly.

The aims of this work are to study the effects of surfactant concentrations and types on synthesized PCB by interfacial polymerization. It is expected to create synthesized PCB with new morphologies and with enhanced electrical conductivity.

4.3 Experimental

4.3.1 Materials

Carbazole (AR grade, Merck) was used as the monomer. Ammonium persulfate (APS) (AR grade, Sigma-Aldrich) was used as the oxidizing agent. Hydrochloric acid 37% and dichloromethane (DCM) (AR grade, RCI Labscan) were used as received as solvents. Cetyltrimethyl ammonium bromide (CTAB), tween 20 (TW20), and sodium dodecyl sulfate (SDS) (AR grade, Sigma-Aldrich), were used as surfactants. Deionized water was used in all experiments.

4.3.2 Polymerization of Polycarbazole

The synthesis procedure of polycarbazole (PCB) followed Gupta *et al.* (2010) using carbazole monomer, APS, hydrochloric acid, and DCM. The

reaction was carried out at 25 °C. The APS (1.2 M) was dissolved in 50 ml of 0.5 M hydrochloric acid solution as an aqueous phase. The carbazole monomer (60 mM) was dissolved in 50 ml of DCM with a surfactant added at various monomer:surfactant mole ratios (the condition are shown in Table 1), to finally obtain a non-aqueous phase. The surfactants used were TW20, CTAB, and SDS. Then, the aqueous and nonaqueous solutions were mixed for 24 h to induce polycarbazole monomers at the interface between the two immiscible phases. After filtering, the green precipitate was collected and dried in oven at 80°C for 24h. Dedoping PCB was performed by stirring the obtained PCB in a solution with the ammonium hydroxide:PCB mole ratio of 1:10 at 25°C for 24h. Then, PCB was doped again by $HClO_4$ at the $HClO_4$ to carbazole (N_{HClO_4}:N_{PCB}) mole ratios of 5:1, 10:1, 50:1, and 100:1.

4.3.3 Characterizations

4.3.3.1 Fourier Transform Infrared Spectrometer

Fourier Transform Infrared Spectrometer, FT-IR (Nicolet, Nexus 670) was used to characterize the functional groups of the synthesized polycarbazole. This technique was used to identify the absorption modes with 32 scans with a resolution of ±4 cm^{-1}, covering a wavelength range of 4000-400 cm^{-1}, using deuterated triglycine sulfate as a detector. Optical grade KBr was used as a background material. The sample was ground with KBr and pressed to form pallets.

4.3.3.2 X-ray Diffractometer

X-ray diffractometer, XRD (Rigaku) was used to investigate the degree of crystallinity in the samples in a based powder form. The diffractometer was operated in the Bragg-Brentano geometry and fitted with a graphite monochromator in the diffracted beam with 5°/min scan rate.

4.3.3.3 Thermal Gravimetric Analyzer

Thermal gravimetric analyzer (DuPont, TGA 2950), was used to characterize thermal properties of the synthesized polycarbazole. The thermal

behavior was investigated by weighting example of 5-10 mg and placed it in a platinum pan, and then heating it under nitrogen flow with the heating rate of 10°C/min from 30-800°C.

4.3.3.4 Scanning Electrŏn Microscope

Scanning Electron Microscope, SEM (Hitachi, S4800) was used to examine the morphological structure of the synthesized polycarbazole and also used to determine dispersion of polycarbazole. The samples were attached on to a brass-stub. Prior to observation, samples were gold sputtered.

4.3.3.5 The Electrical Conductivity

The electrical conductivity of the synthesized polycarbazole was determined by pressing PCB powder into disk pellets using a hydraulic press (diameter of 10 mm and 0.2 mm thick). Electrical conductivity was measured using a custom-built two-point probe meter connected with a voltage supplier, in which voltage was varied and the resultant current measured. The regime where the resultant current is linearly proportional to the applied voltage is called the linear Ohmic regime. The voltage and the current in the Ohmic regime were converted to the electrical conductivity via Equation 4.1:

$$\sigma = 1/\rho = 1/(R_s \times t) = I/(K \times V \times t) \qquad (4.1)$$

where σ is the specific conductivity (S/cm), ρ is the specific resistivity (Ω.cm), R_s is the sheet resistance (Ω/sq), t is the thickness of the sample pellet (cm), V is the applied voltage (V), I is the measured current (A), and K is the geometric correction factor of the two-point probe meter, K as 4.29×10^{-4}. All sample thicknesses were measured by a thickness gauge (Peacock, PDN-20).

4.4 Results and Discussion

4.4.1 Fourier Transform Infrared Spectroscopy

The FT-IR characteristic peaks of synthesized PCB are shown in Figure 4.1 The spectra indicate the successfully synthesized PCB where all the spectra show the same characteristic peaks. The absorbance peaks at 3400 cm^{-1}, 1600-1625 cm^{-1}, 1400-1489 cm^{-1}, 1200-1235 cm^{-1}, 800-875 cm^{-1}, and 700-750 cm^{-1} correspond to the N-H stretching of hetero-aromatics, the C=C stretching of aromatic compound, the C-N stretching of substitutions, the C-H in plane bending, the C-H deformation of tri-substituted benzene ring, and the C-H out-of-plane bending, respectively (Macit *et al.*, 2005, Gupta *et al.*, 2010, Riaz *et al.*, 2013, Zhuo *et al.*, 2013, and Raj *et al.*, 2010). From this result, it can be claimed that the synthesized PCB is not contaminated with any residual surfactant. The proposed mechanism of synthesized PCB is shown in Figure 4.2 (Naddaka *et al.*, 2011).

4.4.2 Thermal Gravimetric Analyzer

The thermal property of PCB, PCB_TW20 (1:0.0068), PCB_CTAB (1:0.0068), and PCB_SDS (1:0.0068) was investigated using TGA to obtain the onset decomposition temperature ($T_{d,onset}$) of the polymer as shown in Figure 3. PCB, PCB_TW20 (1:0.0068), PCB_CTAB (1:0.0068), and PCB_SDS (1:0.0068) show two transition temperatures. The first transition at 400-600 °C ($T_{d,onset}$: 471.69, 485.34, 534.68, and 472.73 °C, respectively) can be assigned to the elimination of PCB small molecules. The second transition at 400-800 °C ($T_{d,onset}$: 731.62, 746.86, 767.08, and 740.34 °C, respectively) can be referred to the decomposition of the polymeric chain (Abthagir *et al.*, 2004). These results also suggest that $T_{d,onset}$ of both transitions increase after adding surfactant. $T_{d,onset}$ of PCB_SDS (1:0.0068) is higher than PCB due to the smaller particle size. $T_{d,onset}$ of PCB_TW20 (1:0.0068) is higher than PCB_SDS (1:0.0068) because of the difference in shapes from hollow sphere to the macroporous honeycomb with a reduced surface area for thermal transport. $T_{d,onset}$ of PCB_CTAB (1:0.0068) is the highest because its shape is a connected hollow microsphere with the highest packing (Figure 4.5). Moreover, the

residue increases with increasing $T_{d,onset}$ because the higher $T_{d,onset}$ provides a shorter time for decomposition and residue formation (Paradee *et al.*, 2013). The residue at $T_{d,onset}$ of the polymeric chain are 18.51, 35.27, 60.85, and 27.47, respectively.

4.4.3 Morphological Structures

4.4.3.1 Effect of Surfactant Types

The morphological structures of the synthesized PCB of the three surfactants (nonionic as TW20, cationic as CTAB, and anionic as SDS), are illustrated in Figure 4. The morphological structures of the synthesized PCB and the synthesized PCB of various surfactant types were obtained at fixed monomer:surfactant mole ratio of 1:0.0068. For the system with no surfactant, the particle shapes are some hollow sphere structures (Figure 4.4 (a)). The systems of TW20, CTAB, and SDS added reveal a macroporous honeycomb structure (Figure 4 (b)), a connected hollow sphere structure (Figure 4.4 (c)), and a small hollow sphere structure (Figure 4.4 (d)), respectively. For the PCB synthesized without surfactant, the formation of the spherical PCB as polymerized by the interfacial polymerization occurs as a vesicle forming from CB monomers (Gupta *et al.*, 2010 and Fuks *et al.*, 2011). Radical CB monomers are formed by the oxidation of the monomers near the interface between HCl and DCM where polymerization takes place initially within the CB micelles (Gupta *et al.*, 2010). The shape of PCB however changes depending surfactant type. For the PCB synthesized with TW20, it produces a macroporous honeycomb structure due to the hexagonal formation of TW20 (Zhou *et al.*, 2010; GruhnTang *et al.*, 2010; Thomas *et al.*, 2013; Garti *et al.*, 2013; Dandan Min *et al.*, 2013; and Edler *et al.*, 2013). The CB monomers were attracted to each hexagonal micelle. For the PCB synthesized with CTAB, it produces a connected hollow sphere structure because the reverse micelles generate some pore spaces within the system and produces a fusion and aggregation of the hollow spheres (Faeder *et al.*, 1984; Preni *et al.*, 1993; Ganguli *et al.*, 2010; and Jhaveri *et al.*, 2013). For the PCB synthesized with SDS, it produces a small hollow sphere due to a vesicle forming from CB micelles. SDS as anionic surfactant reduces micelles which neutralize the charges of CB micelles (Dengand *et al.*, 2010 and Sanchez *et al.*, 2011) and therefore reduces the size of PCB hollow sphere.

4.4.3.2 Effect of Surfactant Concentrations

The morphology of the synthesized PCB (Figure 4.5 (a)) and the synthesized PCB using various surfactant concentrations (CTAB) (Figure 4.5 (b) – 4.5 (d)) reveal the particle shapes as the hollow spheres structure and a connected hollow spheres structure, respectively. For the PCB synthesized without CTAB, the formation of the spherical PCB as polymerized by the interfacial polymerization occurs as the vesicle micelle forming from CB monomers (Gupta *et al.*, 2010). Radical CB monomers are formed by the oxidation of the monomers near the interface between HCl and DCM phases where polymerization takes place initially within the CB micelles (Gupta *et al.*, 2010). For the system with CTAB concentration less than CMC (monomer: CTAB mole ratio of 1:0.0034), it produces a hollow sphere PCB structure similar to the case without CTAB added (Figure 4.5 (b)). At a CTAB concentration lower than CMC, micelle is not fully generated and it has no effect on the packing of PCB. In a system with CTAB concentration equal to CMC (monomer: CTAB mole ratio of 1:0.0068), the CTAB molecules form the reverse micelles (Preni *et al.*, 1993; Keir *et al.*, 1999; Zingaretti *et al.*, 2003; Ganguli *et al.*, 2010; and Jhaveri *et al.*, 2013). The formation of the spherical PCB occurs outside the reverse micelles. The mechanism is however the same as the system without CTAB. So, the reverse micelles generate pore spaces within the system and produce a fusion and aggregation of the hollow spheres (Figure 4.5 (c)). For the system with CTAB concentration at 2 x CMC (monomer:CTAB mole ratio of 1:0.0126), it produces even a higher packing of connected hollow sphere structures (Figure 4.5 (d)) when compared with the system synthesized at CMC (Figure 4.5 (c)). The size of micelle increases with increasing CTAB concentration thus a higher packing of the hollow spherical structures can be expected. Furthermore the polymerization of PCB does not occur at a CTAB concentration more than 2 x CMC.

4.4.4 Electrical Conductivity

Figure 4.6 shows the particle size and electrical conductivity under the effect of CTAB concentrations. When the concentration of CTAB is increased from 1:0 to 1:0.0036 mole ratios, the particle size is decreased, but the electrical

conductivity is slightly increased. When the concentration of CTAB is increased from 1:0.0036 to 1:0.0068 and from 1:0.0068 to 1:0.0136 mole ratios, the particle size is continuously decreased, but the electrical conductivity is greatly increased because the smaller size and higher packing of particles correspond to the higher surface area for electrons to transfer (Paradee *et al.*, 2013).

The electrical conductivity values under the effect of surfactant type (fixed monomer:surfactant mole ratios of 1:0.0068) using three surfactants (nonionic as TW20, cationic as CTAB, and anionic as SDS) and without surfactant are $1.72 \times 10^{-4} \pm 5.80 \times 10^{-6}$ S/cm, $1.00 \times 10^{-3} \pm 7.88 \times 10^{-4}$ S/cm, $2.16 \times 10^{-5} \pm 1.79 \times 10^{-5}$ S/cm, and $2.72 \times 10^{-6} \pm 3.16 \times 10^{-7}$ S/cm, respectively (Table 4.2). The PCB_CTAB has the highest electrical conductivity because it has highest particle packing corresponding to the highest surface area for electrons to transfer. However, PCB_TW20 shows higher electrical conductivity than PCB_SDS because it has a higher surface area for electron transfer. Moreover, the electrical conductivity of all PCB systems of PCB is increased after doping by $HClO_4$. The concentration of $HClO_4$ affects the electrical conductivity; at the polymer:$HClO_4$ ratio of 1:50 it has the highest electrical conductivity (Table 4.2), as this condition is most appropriate for doping to produce an electron withdrawing group. $HClO_4$ pulls an electron out of the polymer backbone. Then, the polymer backbone contains a hole and an electron from a neighboring bond jumps to fill the bond (Permpool *et al.*, 2013). However, PCB_CTAB has the highest electrical conductivity after doping with the polymer:$HClO_4$ ratio of 1:50; the electrical conductivity is increased four orders of magnitude relative to the undoped PCB_CTAB and three orders of magnitude higher than doped PCB. Moreover, all PCB systems synthesized by the interfacial polymerization method have higher electrical conductivity than the sphere particle doped PCB synthesized by the normal chemical polymerization (8.2×10^{-5} S/cm) (Raj *et al.*, 2009), the sphere particle doped PCB synthesized by the electrochemical polymerization (1.27×10^{-4} S/cm) (Abthagir *et al.*, 2004), and the doped PCB film synthesized by the electrochemical polymerization (0.18×10^{-4} S/cm) (Atesa *et al.*, 2015) as shown in table 4.3.

4.5 Conclusions

For the synthesized polycarbazole (PCB), it was synthesized via interfacial polymerization method using carbazole monomer and ammonium persulfate (APS) as the oxidant. The effects of surfactant types and surfactant concentrations on the synthesized PCB were investigated based on the roles of micelle formation.

The particle shape of PCB was changed from the hollow sphere structure to a macroporous honeycomb structure, connected hollow sphere structure, and small hollow sphere structure with the additions TW20, CTAB, and SDS, respectively. The effect of surfactant types (fixed monomer:surfactant mole ratio of 1:0.0136) using the three surfactants (nonionic as TW20, cationic as CTAB, and anionic as SDS) and without surfactant were investigated. The undoped electrical conductivity values were 1.72×10^{-4} S/cm, 1.00×10^{-3} S/cm, 2.16×10^{-5} S/cm, and 2.72×10^{-6} S/cm, respectively. Moreover, the particle packing of the connected hollow sphere increased with increasing CTAB concentration, consistent with the enhanced PCB electrical conductivity. The undoped electrical conductivity of PCB_CTAB at the monomer:surfactant mole ratio of 1:0.0136 was 2.63×10^{-3} S/cm and it increased to 11.3 S/cm when doped at the CB:$HClO_4$ mole ratio of 1:50, the highest electrical conductivity obtained.

4.6 Acknowledgement

The work received financial supports from the Conductive and Electroactive Polymers Research Unit (CEAP) of Chulalongkorn University, the Thailand Research Fund (TRF), and the Royal Thai Government.

4.7 References

Abthagir, P.S. and Saraswathi, R. (2004) Electronic properties of polyindole and polycarbazole Schottky diodes. Organic Electron, 5, 299-308.

Abthagir, P.S. and Saraswathi, R. (2004) Charge transport and thermal properties of polyindole, polycarbazole and their derivatives. Thermochimica Acta, 424, 25–35.

Aditi, M. J. and Vladimir P. T. (2014) Multifunctional polymeric micelles for delivery of drugs and siRNA. Front Pharmacol. 5, 77.

Ashok, K. G, Gangulya, A., and Vaidyaa, S. (2010) Microemulsion-based synthesis of nanocrystalline materials. Chem. Soc. Review, 39, 474-485.

Atesa, M. and Ozyılmazb, A.T. (2015) The application of polycarbazole, polycarbazole/nanoclay and polycarbazole/Zn-nanoparticles as a corrosion inhibition for SS304 in saltwater. Organic Coatings, 84, 50–58.

Deng, M., Jiang, Y., Li, X., Wangab, L., and Liang, H. (2011) Conformational behaviors of a charged-neutral star micelle in salt-free solution. Phys. Chem. Chem. Phys., 12, 6135 – 6139.

Faeder, J. and Ladanyi, B. (1984) Molecular Dynamics Simulations of the Interior of Aqueous Reverse Micelles. A Chem Soci, 13-9.

Fuks, G., Taloma, R.M., and Gauffre, F. (2011) Biohybrid block copolymers: towards functional micelles and vesicles. Chem. Soc. Review, 40, 2475-2493.

Garti, N., Aserin, N., Libster, D., Idit A.Y., Mishraki, T., and Liron, B.C., (2013) Reverse hexagonal mesophases (hii) and uses thereof. Patents, Publication number US20130034538 A1.

Gruhn, T., and Emmerich, H. (2013) Simulation of Stimuli-Responsive Polymer Networks. Chemosensors, 1, 43-67.

Gupta, R. and Prakash, J. (2009) Processible polyacid doped polyaniline composites: Application for charge storage devices. Mater. Sci. Eng., 29, 1746-1751.

Gupta, B., Singh, A.K., and Prakash, R. (2010) Electrolyte effects on various properties of polycarbazole. Thin Solid Films, 519, 1016-1019.

Harun, M.H., Saion, E., Kassim, A., Yahya, N., and Mahmud, E. (2007). Conjugated conducting polymers: A brief overview. JASA, 2, 63-68.

Inselt, G. (2003) Formation and redox behavior of polycarbazole prepared by electropolymerization of solid carbazole crystals immobilized on an electrode surface. Solid State Electrochem, 7, 503-510.

Karen, J. E., and Bin, Y. (2013) Formation of mesostructured thin films at the air–liquid interface. Chem. Soc. Review, 42, 3765-3776.

Keir, R.I., Watson, J.N., and Stradner, A. (1999) Micellisation of metal alkanoates in non-aqueous media. Coll. Surf, 1, 157 - 203.

Kumar, A., and Sinha, J. (2008) Electrochemical transistor for applications in chemical and biological sensing. Organic Semiconductors in Sensor Applications, 22, 246-247.

Min, D., Zhang, X., He, W., Zhang, Y., Li, P., Zhang, M., Liu, J., Liu, S., Xu, F., Dua, Y., and Zhanga, Z. (2013) Direct immobilization of glucose oxidase in magnetic mesoporous bioactive glasses. J. Mater. Chem, 1, 3295 - 3303.

Morin, J.F., Lecrc, M. (1998) Polycarbazoles for plastic electronics. Macromolecules, 34, 4680-4682.

Murat A. (2013) A review study of (bio) sensor systems based on conducting polymers. Materials Science and Engineering, 33, 1853–1859.

Naddaka, M., Mondal, E., Lellouche, J. (2011) Oxidative fabrication of spherical polycarbazole-based microparticles. Oxidative fabrication of spherical polycarbazole-based microparticles, Materials Letters, 65, 1165–1167.

Paradee, N., and Sirivat, A. (2013) Synthesis of poly(3,4-ethylene-dioxythiophene) nanoparticles via chemical oxidation polymerization. Polymer International, 10.1002, 4538-4545.

Peiqin T., and Jingcheng H. (2010) Macroporous honeycomb films of surfactant encapsulated polyoxometalates at air/water interface and their electrochemical properties. Amino Acids, 161, 163–170.

Permpool T., Sirivat A., Aussawasathien D., and Wannatong L., (2004) Development of Polydiphenylamine-Zeolite Y Composite by Dealumination Process as a Sensing Materials for Halogenated Solvents. Polym Plast Technol Eng, 52, 907-920.

Raj, V., Madheswari, D., and Ali, M. (2010) Chemical formation, characterization and properties of polycarbazole. Applied Polymer Science, 116, 147-154.

Rani, K.S.V., and Santhanam, J. (1998) Interfacial polymerization of carbazole: Morphology controlled synthesis. Solid state electrochem, 2, 999-1004.

Sancheza, R and Bartlett, P. (2011) Synthesis of charged particles in an ultra-low dielectric solvent. Soft Matter, 7, 887-890.

Saxena, V., Shirodkar, R., and Prakash, J. (2008) Room temperature operated ammonia gas sensor using polycarbazole Langmuir–Blodgett film. Sensors and Actuators B: Chemica, 4, 234-236.

Tran-Van, F., Henri, T., and Chevrot, C. (2002) Synthesis and electrochemical properties of mixed ionic and electronic modified polycarbazole. Electrochimica Acta, 47, 2927 – 2936.

Tungkavet, T., Seetapan, N., Pattavarakorn, D., and Sirivat, A. (2012) Improvements of electromechanical properties of gelatin hydrogels by blending with nanowire polypyrrole: effects of electric field and temperature. Polymer International, 61, 825–833.

Ufana, R., and Ashraf, S.M. (2011) Effect of solid state intercalation conditions in controlling the self-assembled nanostructured polycarbazole–montmorillonite nanocomposites synthesized by mechano-chemical and microwave-assisted techniques. Applied Clay Science, 52, 179–183.

Zingaretti L., Boscatto L., Chiacchiera M., and Silber J. (2003) Kinetics and mechanism for the reaction of 1-chloro-2,4-dinitrobenzene with n-butylamine and piperidine in AOT/n-hexane/water reverse micelles. Arkivoc, 34, 189-200.

Zhou, W., Gu, T., Su, Z., and Ma. G. (2010) Synthesis of macroporous poly(glycidyl methacrylate) microspheres by surfactant reverse micelles swelling method. European Polymer, 43 4493–4502.

Zhuo, Y., Du, C., Li, X., Sun, W., and Ying Chu, Y. (2013) One-step synthesis and photoluminescence properties of polycarbazole spheres and Ag/polycarbazole core/shell composites. European Polymer, 1365–1372.

Table 4.1 The synthesizing conditions of PCB by interfacial polymerization with various types and concentrations of surfactant at polymerization time of 24 h

Surfactant Types	**Monomer : Surfactant (Mole Ratio)**	**Remark**
None	1:0	PCB
Tween 20 (nonionic)	1:0.0034	PCB_TW20 (1:0.0034)
	1:0.0068	PCB_TW20 (1:0.0068)
	1:0.0136	PCB_TW20 (1:0.0136)
	1:0.0272	-
CTAB (cationic)	1:0.0034	PCB_CTAB (1:0.0034)
	1:0.0068	PCB_CTAB (1:0.0068)
	1:0.0136	PCB_CTAB (1:0.0136)
	1:0.0272	-
SDS (anionic)	1:0.0034	PCB_SDS (1:0.0034)
	1:0.0068	PCB_SDS (1:0.0068)
	1:0.0136	PCB_SDS (1:0.0126)
	1:0.0272	-

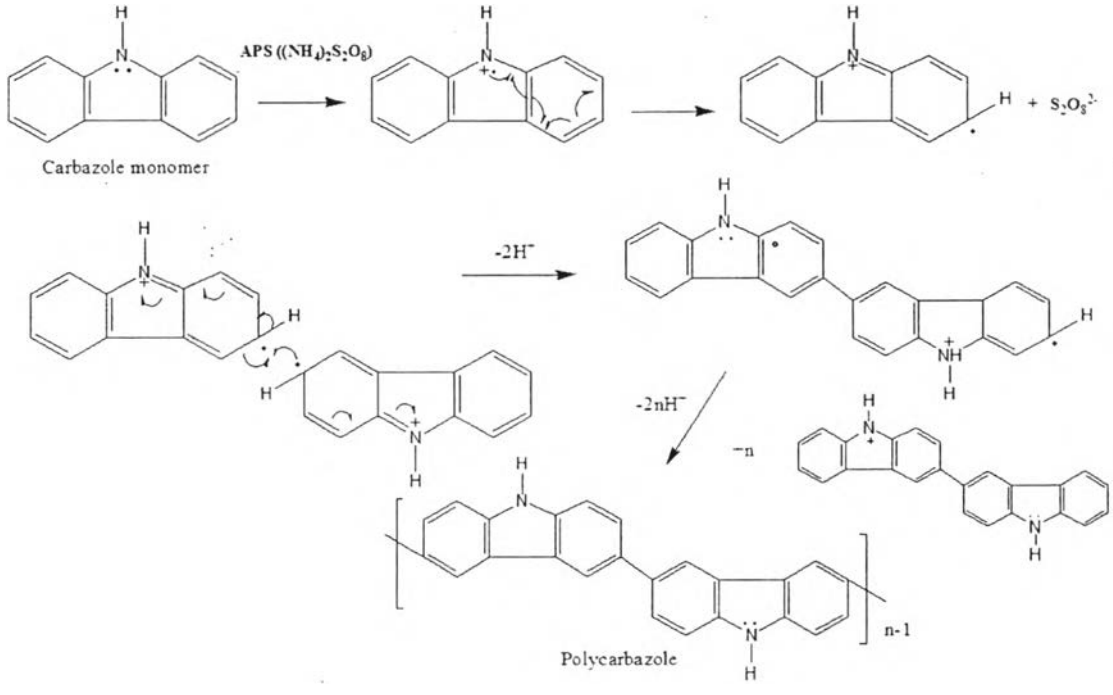

Figure 4.1 Proposed mechanistic scheme for the polymerization of PCB.

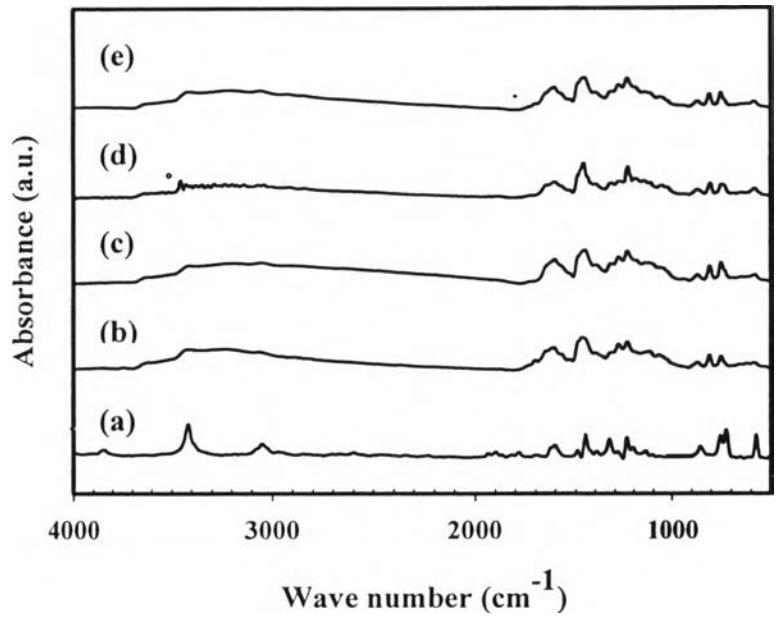

Figure 4.2 The FTIR spectra of PCB with interfacial polymerization synthesized by various surfactant types: (a) PCB_monomer; (b) PCB; (c) PCB_TW20 (1:0.0068); (d) PCB_CTAB (1:0.0068); and (d) PCB_SDS (1:0.0068).

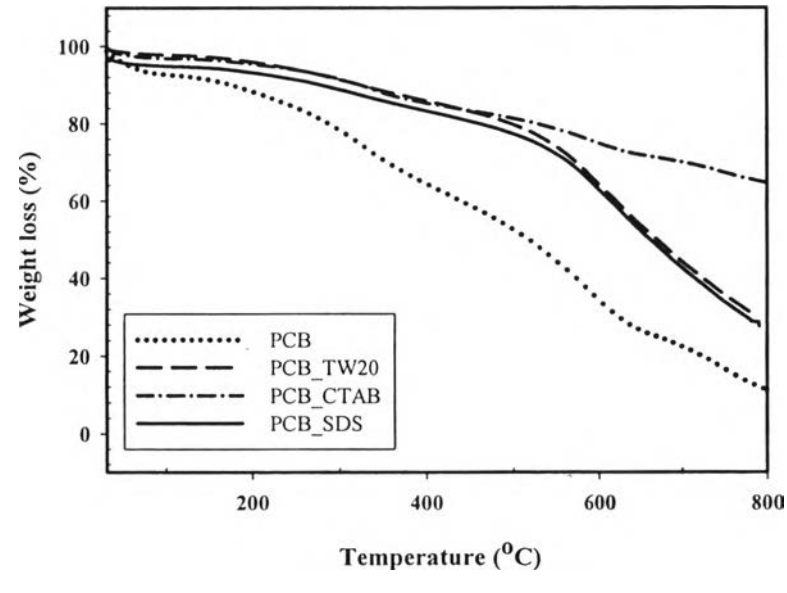

Figure 4.3 TGA thermograms of PCB with interfacial polymerization synthesized by various surfactant types.

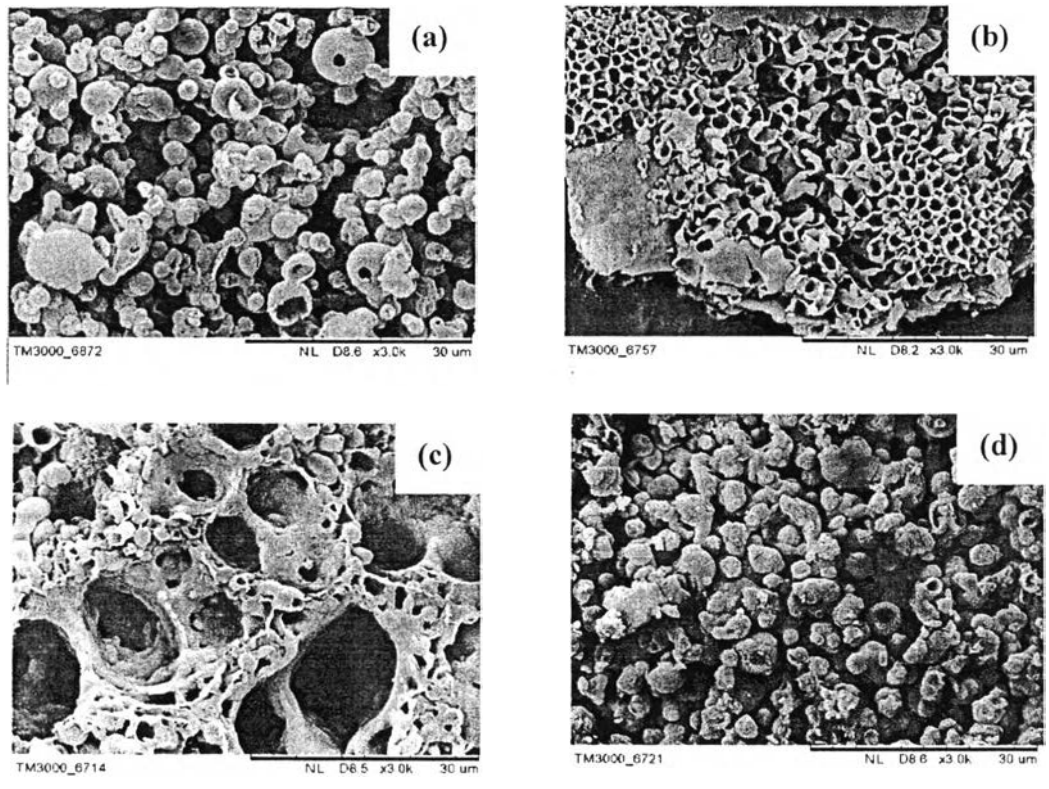

Figure 4.4 SEM photographs of PCB synthesized by interfacial polymerization with different surfactant types: (a) PCB; (b) PCB_TW20 (1:0.0068); (c) PCB_CTAB (1:0.0068); and (d) PCB_SDS (1:0.0068) at 24 h).

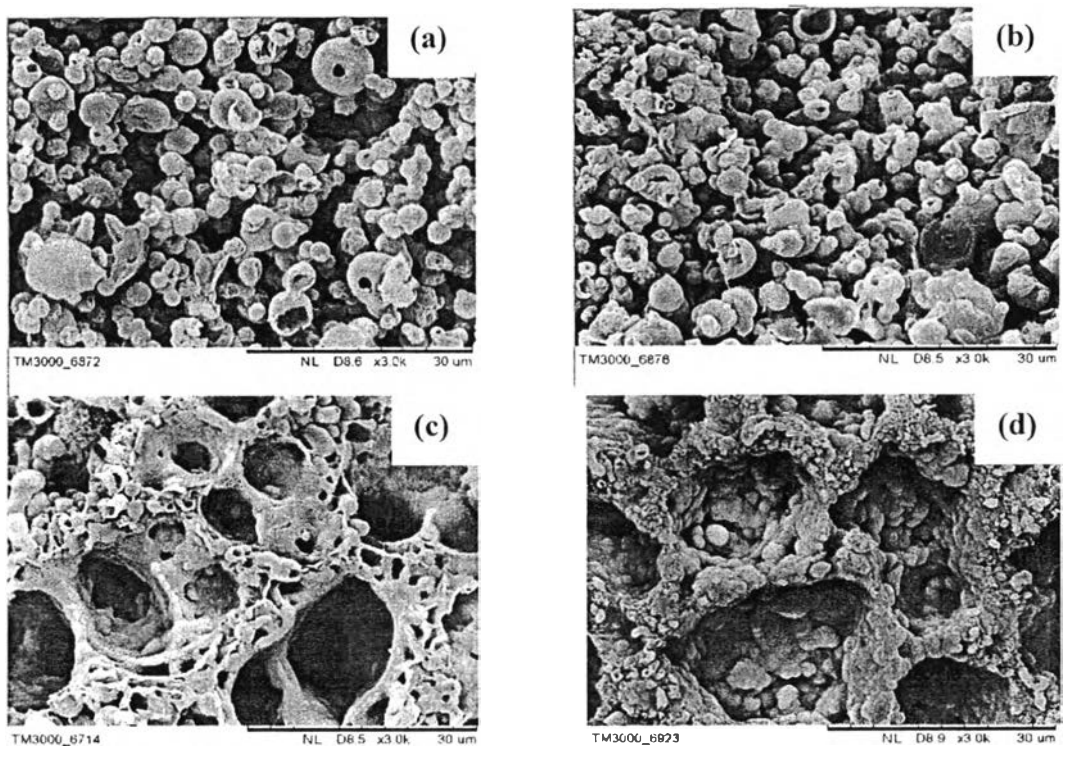

Figure 4.5 SEM photographs of PCB synthesized by interfacial polymerization at various monomer: CTAB mole ratios: (a) PCB:CTAB (1:0), (without CTAB); (b) PCB:CTAB (1: 0.0034), (less than CMC; (c) PCB:CTAB (1:0.0068), (at CMC); and (d) PCB:CTAB (1:0.0136), (more than 2 x CMC) at 24 h.

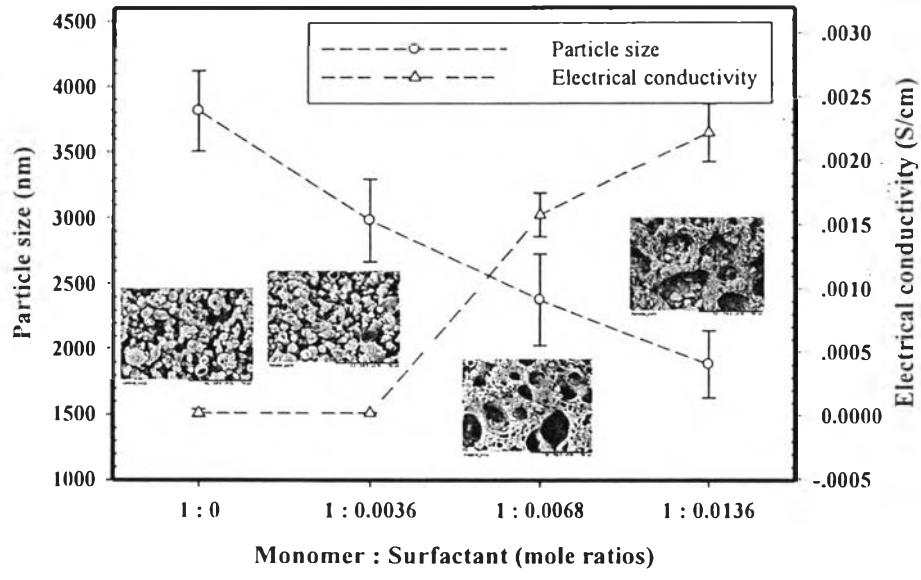

Figure 4.6 The particle size and electrical conductivity of PCB with interfacial polymerization synthesized by various CTAB concentrations.

Table 4.2 Particle size and electrical conductivity of PCB with various surfactant types

Samples	Particle Size (nm)	Electrical Conductivity (S/cm)	
		Undoped	Doped
PCB	3213 ± 944	2.72E-06 ± 3.16E-07	5.59E-02 ± 2.69E-03
PCB_TW20 (1 : 0.0136)	1182 ± 327	1.72E-04 ± 5.80E-06	7.67E-01 ± 3.70E-02
PCB_CTAB (1 : 0.0136)	2068 ± 455	2.62E-03 ± 7.88E-04	1.13E+01 ± 3.61E-01
PCB_SDS (1 : 0.0136)	2841 ± 835	2.16E-05 ± 1.79E-05	4.49E-02 ± 3.32E-03

Table 4.3 Comparison of particle size and electrical conductivity of doped PCB

Samples	Morphology	Electrical Conductivity (S/cm)	Reference
Doped PCB	Hollow sphere	5.59×10^{-2}	-
Doped PCB_TW20	Macroporus honeycomb	7.67×10^{-1}	-
Doped PCB_CTAB	Connected hollow sphere	11.3	-
Doped PCB_SDS	Small hollow sphere	4.49×10^{-2}	-
Doped PCB	Sphere	8.20×10^{-5}	Raj *et al.*, 2009
Doped PCB	Sphere	1.27×10^{-4}	Abthagir *et al.*, 2004
Doped PCB	Sphere	0.18×10^{-4}	Atesa *et al.*, 2015